7-2-2007

Electromagnetically Induced Transparency Line Shapes for Large Probe Fields and Optically Thick Media

M. V. Pack
University of Rochester

R. M. Camacho
University of Rochester

John C. Howell
Chapman University, johhowell@chapman.edu

Recommended Citation

M. V. Pack, R. M. Camacho, and J. C. Howell,*Electromagnetically Induced Transparency Line Shapes for Large Probe Fields and Optically Thick Media*, Phys. Rev. A **76**(1), 013801.

Electromagnetically Induced Transparency Line Shapes for Large Probe Fields and Optically Thick Media

Electromagnetically induced transparency line shapes for large probe fields and optically thick media

M. V. Pack, R. M. Camacho, and J. C. Howell*
Department of Physics, University of Rochester, Rochester, New York 14627, USA
(Received 9 November 2006; published 2 July 2007)

We calculate the line shape and linewidths for electromagnetically induced transparency (EIT) in optically thick, Doppler broadened media (buffer gasses are also considered). In generalizing the definition of the EIT linewidth to optically thick media, we find two different linewidth definitions apply depending on whether the experiment is pulsed or continuous wave (cw). Using the cw definition for the EIT line shape we derive analytic expressions describing the linewidth as a function of optical depth. We also review the EIT line shapes in optically thin media and provide physical arguments for how the line shapes change as a function of various parameters.

DOI: 10.1103/PhysRevA.76.013801 PACS number(s): 42.50.Gy, 32.70.Jz

I. INTRODUCTION

Electromagnetically induced transparency (EIT) is an important component for numerous experiments spanning the subjects of slow light [1–3], stored light [4,5], generation of correlated photon pairs [6], quantum information processing [7] EIT-enhanced nonlinear optics such as frequency mixing or generation [8–12], magnetometry [13–15], atomic frequency standards [15–17], phase conjugate optics [18], and Kerr nonlinearities [19–21]. Understanding the shape of the transparency is important for many of these experiments. For example, in slow-light experiments the EIT line shape determines the group velocity and pulse broadening [22]. Also, the rise time of EIT Kerr nonlinearities is inversely proportional to the EIT linewidth [23].

Although EIT can be realized in many different circumstances (e.g., solid state systems [24] and hot or cold atomic vapors), we focus our discussion on EIT in Λ-type, hot atomic vapors. However, our treatment is rather general and may be generalized to other inhomogeneously broadened systems.

There has already been a great deal of work towards understanding EIT line shapes [15,25–35], and there are several reviews of EIT and coherent population trapping [36–39]. However, most of the work on EIT line shapes is limited to EIT in optically thin media and most research assumes that one of the EIT fields is much stronger than the other (the weak field is called the probe and the strong field is called the coupling field) [29–35,40]. For many applications of EIT it is desirable to violate these assumptions and to use optically thick media and/or large probe fields. The definition of "large" probe field varies depending on the situation, but in general the probe field is large when the small probe assumption used in perturbative calculations becomes inaccurate. The probe Rabi frequency is always assumed to be smaller than the coupling Rabi frequency.

Simple models for the EIT line shapes, which assume a single homogeneous line and a three-level system, have been well understood for many years [36,38,41]. Recently more complete and experimentally realistic models for EIT line shapes have been studied. These models include Doppler broadened systems [29,31–33,40] and systems with buffer gasses [30,34,35]. Other studies have looked at how the optical density of the medium influences the EIT line shape via effects such as radiation trapping [42–44] or nonlinear optical interactions [28]. (Note that optically dense does not imply optically thick and vice versa.)

Some research already exists related to EIT in optically thick media. For example, Rochester *et al.* have studied how nonlinear magneto-optical rotation in optically thick media differ from the optically thin media [45]. Also, Godone *et al.* have reported narrowing of the EIT linewidth for optically thick ^{87}Rb vapor in a buffer gas [46–48]. The Godone *et al.* experiments were directed towards improving frequency standards and used a longitudinal magnetic field to resolve only the dark-line associated with the clock states (i.e., $m_F=0$ ground states) [46–48]. There is still more to be understood about the effects of optical thickness on EIT line shapes and linewidths especially for Doppler broadened EIT systems.

In this paper we study the effects of optical thickness on EIT line shapes (by optically thick we mean $\alpha L \gg 1$, where α is the absorption coefficient and L is the length of the medium). However, we do not discuss optical dense media in which radiation trapping and coherent interactions between atoms such as super-radiance or coherent Raman scattering play a role. Many experiments such as slow-light and EIT Kerr measurements require large optical thickness in order to achieve measurable effects, and for optically thick media the EIT line shape often differs significantly from the optically thin EIT line shape. The differences between optically thick and thin media arise because in optically thick media the fields are attenuated as they transverse the medium, and EIT line shapes are strongly dependent on the field intensities.

This paper is divided into two parts. First, Sec. II discusses the various optically thin EIT line shapes encountered in common experimental circumstances. Then in Sec. III we use the functional forms of the optically thin EIT line shapes to calculate the optically thick EIT line shapes. Although much of Sec. II is a review of well known results, we have

*Electronic address: mvpack@pas.rochester.edu

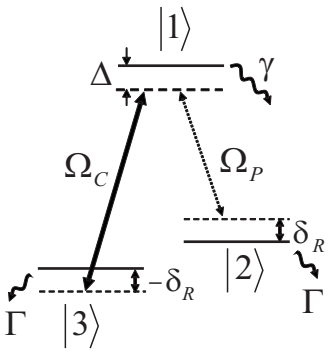

FIG. 1. Diagram of a three-level Λ-type atom with a strong coupling field and a weak probe field. The detunings are defined as $\Delta=(\Delta_P+\Delta_C)/2$ and $\delta_R=\Delta_P-\Delta_C$, where $\Delta_P=(\omega_1-\omega_2)-\omega_P$ and $\Delta_C=(\omega_1-\omega_3)-\omega_C$. Also, the Rabi frequencies are defined as $\Omega_i=\mu_i E_i/\hbar$, where $i=\{P,C\}$ (signifying probe and coupling fields, respectively), the dipole moments μ_i are assumed to be real, and E_i is the electric field. The spontaneous emission rate out of the excited state is given by γ and the ground state decoherence rate Γ is the same for both ground states.

tried to present the results in novel, physically intuitive, and mathematically simple ways. All of Sec. III is new.

II. OPTICALLY THIN EIT LINE SHAPES

To calculate the EIT line shapes in optically thick media we must first understand EIT line shapes in optically thin media. Different systems exhibit different EIT line shapes. For example, EIT in homogeneously broadened systems, such as a cold atomic gas with a single-velocity class, will have an approximately Lorentzian line shape near single-photon resonance. Whereas, the EIT line shape in a Doppler broadened atomic vapor will be either *V* shaped or *U* shaped depending on the relative strengths of the probe field (see Fig. 5). Also, the EIT line shapes can depend on other factors such as whether or not the atoms experience velocity-changing, coherence-preserving collisions (VCCPCs).

In this section we discuss the line shapes and linewidths for three-level EIT systems such as the one shown in Fig. 1 under different conditions, such as Doppler broadening and VCCPC. Many of the optically thin results discussed here can also be found elsewhere, but it is helpful to establish a single uniform notation. Also, we try to emphasize the physics while minimizing the complexity of the mathematical expressions. Readers already familiar with EIT line shapes in optically thin media may want to skip to Sec. III.

A. Single velocity class line shapes

First, let us consider the line shape of a Λ-EIT system with a single homogeneous line (see Fig. 1). Although this problem is well understood and its solution can be found in numerous text books [38,41] it deserves some consideration here as it will be the basis for understanding the EIT line shapes of Doppler broadened systems.

Figure 1 shows a prototypical three-level EIT system with a strong coupling field (Rabi frequency Ω_C) and a weak probe field (Rabi frequency Ω_P). The figure caption defines the detunings and decoherence rates associated with this system. The three-level system is assumed to be a closed system with all decay out of any given state incoherently repopulating another state. When the two-photon detuning δ_R is zero the system becomes trapped in the dark state $|-\rangle=(\Omega_P|3\rangle-\Omega_C|2\rangle)/\Omega$, which is decoupled from the excited state making the medium transparent. We also define the bright state $|+\rangle$ as the superposition of ground states orthonormal to the dark state (i.e., $\langle+|-\rangle=0$) and the coupling between the bright state and excited state is given by the bright Rabi frequency $\Omega=\sqrt{\Omega_P^2+\Omega_C^2}$.

The dynamics of this system are governed by the master equation

$$\dot{\rho}=\frac{1}{i\hbar}[H,\rho]-D, \tag{1}$$

where the coherent evolution is determined by the Hamiltonian

$$H=\begin{pmatrix} \Delta & -\frac{\Omega_P}{2} & -\frac{\Omega_C}{2} \\ -\frac{\Omega_P^*}{2} & -\delta_R/2 & 0 \\ -\frac{\Omega_C^*}{2} & 0 & \delta_R/2 \end{pmatrix}. \tag{2}$$

The decoherence matrix is

$$D=\begin{pmatrix} \gamma\rho_{11} & \gamma_\perp\rho_{12} & \gamma_\perp\rho_{13} \\ \gamma_\perp\rho_{21} & \Gamma(\rho_{22}-\rho_{33})-\frac{\gamma}{2}\rho_{11} & \Gamma_\perp\rho_{23} \\ \gamma_\perp\rho_{31} & \Gamma_\perp\rho_{32} & \Gamma(\rho_{33}-\rho_{22})-\frac{\gamma}{2}\rho_{11} \end{pmatrix}, \tag{3}$$

and the spontaneous emission at rate γ repopulates both ground states with equal probability (i.e., the dipole moments are equal $\mu_P=\mu_C$), $\gamma_\perp=(\gamma+\gamma'+\Gamma)/2$ is the transverse decoherence rate for the excited state coherences, and $\Gamma_\perp=(\Gamma'+\Gamma)$ is the decoherence rate for the ground state coherence. The primed decoherence rates γ' and Γ' are the dephasing rates for the coherences, and are assumed to be zero unless explicitly stated otherwise. Additionally, throughout this paper we assume that the Rabi frequencies are real and that $\gamma \gg \Gamma$, such that $\gamma_\perp \approx \gamma/2$, unless stated otherwise.

In its most general form the steady state analytic solution of Eq. (1) is so complicated that it provides little insight, which is why approximate solutions for the EIT line shape are widely used [31,36–39,41]. We discuss two different approximation methods. First, in Appendix A we use perturbation theory to solve Eq. (1) to first order in Ω_P and to all orders in all other parameters (this is probably the most common solution method for these types of problems, see Refs. [31,38,41]). The simplicity of this solution makes it ideal for gaining intuition, but the perturbative solution is only valid in the limit that the probe field is weak. Also, when the

single-photon detuning is large, as is the case for certain velocity classes in Doppler broadened systems, the probe Rabi frequency must be several orders of magnitude smaller than the coupling Rabi frequency in order to use the perturbative solution (see Appendix A for details).

A more general derivation of EIT line shapes uses what we call the Bloch-vector method, and this derivation makes no assumptions about the relative strengths of the probe and coupling fields (see Appendix B and Ref. [11]). This method assumes only that the excited state coherences can be adiabatically eliminated, an assumption that is strengthened when the single-photon detuning is large. Thus, the Bloch-vector method is ideal for calculating EIT line shapes in Doppler broadened media.

For the case of zero decoherence ($\Gamma=0$) the perturbative solution gives a probe susceptibility of

$$\chi_P^{(a)}(\delta_R) = \frac{N\mu_p^2}{2\hbar\epsilon_0}\rho_{12} \approx \alpha_0 \frac{2\delta_R}{\Omega_C^2/\gamma + 4\Delta_P\delta_R/\gamma - 2i\delta_R}, \quad (4)$$

where $\alpha_0=N|\mu_p|^2/2\hbar\epsilon_0\gamma$ is the incoherent probe absorption coefficient, N is the atomic number density, $\gamma'=0$, and the other constant have their typical meanings (see Appendix A for the derivation). Although Eq. (4) was derived assuming $\Gamma=0$, this solution is also a good approximation for the case $\Gamma\neq 0$ so long as the EIT condition $\Omega_C^2\gamma/(4\Delta^2+\gamma^2)\gg\Gamma$ is satisfied. For simplicity we assume $\gamma\gg\Omega_C$.

Near single-photon resonance the transparency resonance has a Lorentzian line shape with a full width at half maximum (FWHM) of $\Gamma_{\mathrm{EIT}}=\Omega_C^2/\gamma+2\Gamma$. Physically this can be understood as the detailed balancing between pumping out of the dark state and pumping into the dark state. For continuous wave (cw) EIT, optical pumping is the primary mechanism transferring atoms from the bright state to the dark state, and the optical pumping ratio R from the bright state to the dark state is calculated by taking the product of the probability that an atom has been excited from the bright state $P(|+\rangle\rightarrow|1\rangle)$ times the spontaneous emission rate from the excited state into the dark state, which is $\gamma/2$, i.e.,

$$R = \frac{\gamma}{2}P(|+\rangle\rightarrow|1\rangle),$$

where

$$P(|+\rangle\rightarrow|1\rangle) = \frac{\mathrm{Tr}(\rho|1\rangle\langle 1|)}{\mathrm{Tr}[\rho(|+\rangle\langle +|+|1\rangle\langle 1|)]} = \frac{\Omega^2/2}{\Omega^2+\Delta^2\gamma/\gamma_\perp+\gamma\gamma_\perp}.$$

Near resonance the optical pumping rate simplifies to $R\approx\Omega^2/4\gamma_\perp$, if the fields are well below saturation intensities.

The transfer rate out of the dark state is due to the decoherence Γ and Raman detuning δ_R. Thus, the total pumping rate out of the dark state is

$$R_\Gamma \approx \Gamma_\perp + \delta_R^2/R. \quad (5)$$

In Eq. (5) we have assumed the EIT condition $R\gg\Gamma_\perp$, and we have assumed $\rho_{22}\approx\Omega_C^2/\Omega^2$ and $\rho_{33}\approx\Omega_P^2/\Omega^2$, which are both valid assumptions under normal EIT conditions. Applying detailed balancing subject to the constraints $\rho_{22}=\Omega_C^2/\Omega^2$ and $\rho_{33}=\Omega_P^2/\Omega^2$, we see that the EIT absorption line is approximately

$$\alpha L \propto \frac{R_\Gamma}{R+R_\Gamma}. \quad (6)$$

This is simply a Lorentzian transparency resonance with linewidth $\Gamma_{\mathrm{EIT}}=\Omega_C^2/2\gamma_\perp+2\Gamma_\perp$, and is in excellent agreement with Eq. (4). Also, we see that the EIT condition can be stated as the pumping rate into the dark state R must be much larger than the pumping rate out of the dark state on Raman resonance $R_\Gamma(\delta_R=0)$.

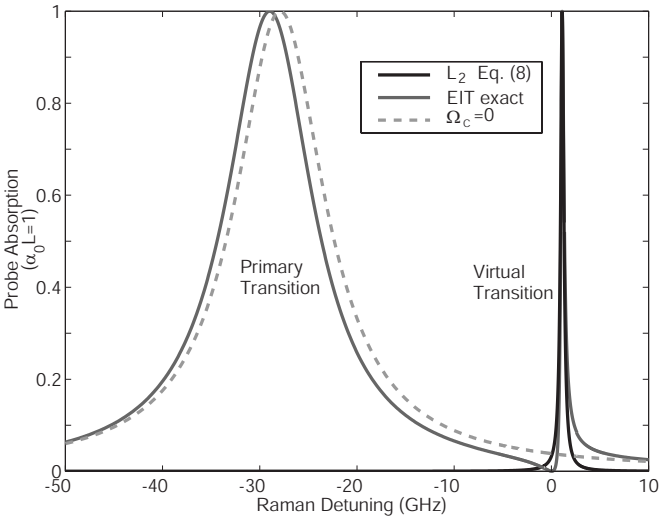

FIG. 2. EIT in the far detuned case. Grey solid line shows the probe absorption for EIT when $\gamma=2\pi\times 6$ MHz and $\Delta_C=5\gamma$. The dashed gray curve shows the probe absorption in the absence of a coupling field, and the black solid line shows the probe absorption for a virtual transition as calculated in Eq. (8).

The EIT line shape changes dramatically as the single-photon detuning is moved far from single-photon resonance $\Delta\gg\gamma$. In this case the dominant feature of the EIT line is not the transparency near Raman resonance, but a virtual absorption line slightly to one side Raman resonance as shown in Fig. 2. The physics of this process is best understood in the dressed state picture in which the atom is dressed by the coupling field. In the dressed state picture the excited state energy level is split into two energy levels. The primary energy level which is the original excited state that has been Stark shifted by $\Omega_C^2/4\Delta_C$, and it has an absorption line shape given by

$$L_1(\delta_R) = \frac{\alpha_0 L\gamma^2\tilde{\rho}_{gg}^2}{(\delta_R+\Delta_C+\Omega_C^2/4\Delta_C)^2+\gamma^2\tilde{\rho}_{gg}^2}. \quad (7)$$

The secondary or virtual energy level is near $\delta_R=0$, and its absorption shape is given by

$$L_2(\delta_R) = \frac{\alpha_0 L\gamma^2\tilde{\rho}_{ee}^2}{(\delta_R-\Omega_C^2/4\Delta_C)^2+\gamma^2\tilde{\rho}_{ee}^2}, \quad (8)$$

where $\tilde{\rho}_{ee}=\Omega_C^2/4\Delta_C^2$ and $\tilde{\rho}_{gg}=1-\tilde{\rho}_{ee}$. Although the dressed state picture does not specifically address the interference

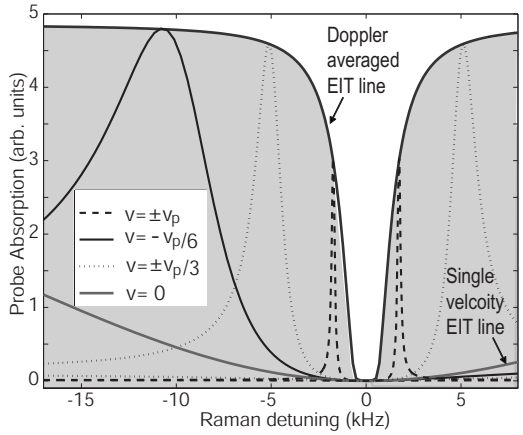

FIG. 3. Probe absorption versus Raman detuning for a Doppler averaged EIT line shape and the probe absorption for several different velocity classes which contribute to the Doppler averaging. The parameters used to calculate these absorption curves are $\Gamma=0$, $\gamma=\approx 2\pi\times 6$ MHz, $v_p=50c\gamma/\omega_0=222$ m/s.

responsible for EIT, transparency can be mimicked near Raman resonance by combining L_1 and L_2 to create

$$L_{\text{total}}=[\sqrt{L_1(\delta_R)}-\sqrt{L_2(\delta_R)}]^2, \tag{9}$$

where the minus sign simulates the interference responsible for EIT. Figure 2 shows the agreement between Eq. (8) and the exact steady state solution of Eq. (1).

When the single photon detuning is large, i.e., $\Delta \gg \gamma$, the transparency region near $\delta_R=0$ will be broad and flat compared to the sharp narrow absorption spike due to the virtual transition (see Fig. 3, for example). The virtual transition is centered at

$$\delta_R=\delta_{VC}=\Omega_C^2/4\Delta_C\approx 2\Delta R/\gamma, \tag{10}$$

and has a FWHM of $\gamma\Omega_C^2/2\Delta^2\approx 4R$, where we assume $\Delta \approx \Delta_C$, and where the subscript "*VC*" stands for virtual transition center. The transparency region is much larger than the virtual transition with a half width at half maximum (HWHM) of approximately $2\Delta R/\gamma$, which is a factor of Δ/γ larger than the absorption HWHM. The asymmetric line shape of the transparency region makes defining a transparency linewidth somewhat ambiguous, so we choose to define the far-detuned EIT HWHM as the frequency difference between Raman resonance $\delta_R=0$ and the Raman detuning at the half-maximum of the virtual transition. When $\Delta/\gamma\gg 1$ the virtual transition is sufficiently narrow that it can be approximated as Dirac delta function; a fact that we exploit in Appendix B.

As mentioned earlier the perturbative solution does not converge when both the single-photon detuning $\Delta \gg \gamma_\perp$ and the probe field are large $\Omega_P\sim\Omega_C$. In this case the Bloch vector method must be used and the virtual transition from Eq. (8) is modified to become

$$L_2(\delta_R)=\frac{\alpha_0 L\gamma^2\tilde{\rho}_{ee}^2}{(\delta_R-\mathcal{F}\Omega_C^2/4\Delta_C)^2+\gamma^2\tilde{\rho}_{ee}^2\mathcal{F}^2}, \tag{11}$$

where $\mathcal{F}=\sqrt{1+\Omega_P^2\gamma_\perp^2/\Delta^2\Omega_C^2}$ (see Appendix B). Finally, in both Eq. (11) and Eq. (8) we have assumed $\Gamma=0$. This assumption is justified so long as the EIT condition is satisfied. However, when the EIT condition is not satisfied and the $\Delta \gg \gamma$ the virtual transition absorption is modified such that Eq. (8) should become

$$L_2(\Gamma\neq 0)\approx\frac{2R^2L_2(\Gamma=0)}{(\sqrt{2}R+\Gamma)^2}. \tag{12}$$

B. Doppler broadened atomic systems

In hot atomic vapors, atoms with different velocities will experience different Doppler shifts resulting in an inhomogeneously broadened absorption line. Doppler broadening also effects the EIT line shapes making the linewidth substantially narrower and the line shape typically deviates significantly from the single-velocity Lorentzian line shape.

The EIT linewidths for Doppler broadened systems have been derived for the cases of weak probe fields in Refs. [31,33] and for large probe fields in Ref. [29], but these studies focused on the linewidth largely ignoring the line shape. We discuss both the linewidths and line shapes here because the line shapes are also important for determining the linewidths in optically thick media. We restrict our discussion to Λ EIT systems with copropagating beams (these results are similar to ladder EIT systems with counter propagating beams).

In Doppler averaged systems the total susceptibility is found by integrating over the susceptibility of each velocity class:

$$\chi_P=\int_{-\infty}^{\infty}dv\,\chi_P(v)\frac{\exp(-v^2/2v_p^2)}{v_p\sqrt{2\pi}}, \tag{13}$$

where $v_p=\sqrt{2k_BT/m}$ is the most probable velocity in the Maxwellian velocity distribution, and m is the atomic mass. Also, the velocity dependence of $\chi_p(v)$ is implicitly contained in the detunings $\Delta_p(v)=\Delta_p(0)+v\omega_0/c$ and $\delta(v)=\delta(0)+v\Delta_{23}/c$, where Δ_{23} is the frequency difference between levels $|2\rangle$ and $|3\rangle$. For the remainder of the paper we assume that the ground state energies are degenerate, i.e., $\Delta_{23}=0$, unless explicitly stated otherwise. Note, an approximate analytic solution for the imaginary part of Eq. (13) is derived in Eq. (B15) from Appendix B.

Figure 3 shows how Doppler averaging results in narrower EIT linewidths, and how these narrower line shapes, deviate from Lorentzian. The solid gray curve near the bottom of Fig. 3 shows the absorption due to a the velocity class $v=0$. This single-velocity line shape is so broad that it extends well beyond the bounds of the figure. In contrast, the Doppler averaged absorption curve is much narrower. The virtual transition associated with $v=\pm v_p/6$, $v=\pm v_p/3$, and $v=\pm v_p$ are also plotted to illustrate how the superposition of virtual transitions for the far detuned velocity classes combine to fill in the wings of the $v=0$ transparency resonances.

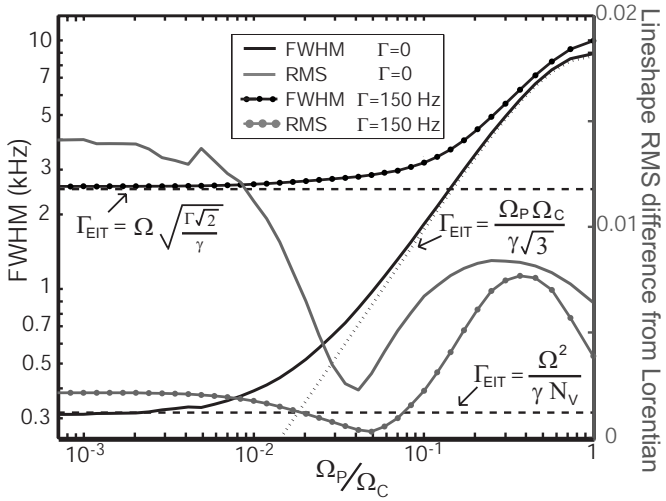

FIG. 4. EIT linewidth (solid black lines) versus the ratio of Rabi frequencies Ω_P/Ω_C. The gray lines plot the root mean square difference between the EIT line shape and a Lorentzian line of the same size and FWHM versus the ratio of Rabi frequencies. The dashed lines show the asymptotic values of the linewidths, and the analytic expressions for these asymptotic values are also given. (Note: $\gamma N_V = \Delta_D$).

The farthest detuned velocity classes have absorption peaks nearest Raman resonance (e.g., the $v = \pm v_p$ velocity classes in Fig. 3), and these velocity classes contribute most strongly to the narrowest part of the Doppler broadened EIT line shape. Thus, the Doppler broadened line shapes can be well understood simply by studying the factors influencing the virtual transitions of the off-resonant velocity classes (this is not true for VCCPC systems which are discussed later).

Figure 4 shows how the EIT linewidths and line shapes change as a function of the ratio between probe and coupling Rabi frequencies $|\Omega_P|/|\Omega_C|$. These curves were obtained by numerically integrating Eq. (13) with $\chi_P(v)$ being the exact steady state solution of Eq. (1). The two solid gray curves are associated with the gray vertical axis on the right, and show the root mean square (rms) difference between the EIT line shape and a Lorentzian line shape of the same height and width. All black curves (solid, dashed, or dotted) are linewidths (FWHM) and are associated with black vertical axis on the left. All data is plotted versus the ratio between probe and coupling Rabi frequencies Ω_P/Ω_C, with the bright Rabi frequency $\Omega = \sqrt{\Omega_P^2 + \Omega_C^2}$ held constant. Also, for the plots in Fig. 4 the ground state decoherence rates were $\Gamma = 0$ and $\Gamma = \Omega^2/100\gamma = 2\pi \times 150$ Hz as indicated in the figure legend.

In both the large- or weak-probe limits it is possible to find asymptotic expressions for the linewidth and line shape. The asymptotic values for the weak-probe linewidth are shown by the dashed black lines in Fig. 4, and large-probe asymptotic linewidth is the dotted curve. These asymptotic solutions are easiest to understand by thinking about the far-detuned velocity classes and Eq. (12).

First, consider the weak-probe limit, in which case the linewidth asymptotically approaches

$$\Gamma_{\mathrm{EIT}}^{WP} \approx \frac{\Omega^2}{\tilde{\Delta}}, \tag{14}$$

where the effective inhomogeneous linewidth $\tilde{\Delta}$ is given by

$$\frac{1}{\tilde{\Delta}} = \sqrt{\frac{1}{\Delta_D^2} + \frac{\Gamma\sqrt{2}}{\Omega^2\gamma}} \tag{15}$$

and $\Delta_D = \sqrt{8 \ln 2} v_p \omega_0 / c$ is the inhomogeneous Doppler broadened FWHM. In the weak-probe limit the functional form for the line shape is

$$\alpha^{(WP)}(\delta_R) \propto \exp(-\ln 2\Omega^4/4\delta_R^2\tilde{\Delta}^2), \tag{16}$$

which is a U shape, and is derived in Eq. (B16) of Appendix B. On single-photon resonance, i.e., $\Delta(v=0)=0$, the farthest detuned velocity class contributing to the EIT line shape has a detuning of about $\tilde{\Delta}/2$ (velocity classes with larger detunings do not satisfy the EIT condition). The EIT FWHM is approximately

$$\Gamma_{\mathrm{EIT}} \approx \delta_{VC}(\Delta = \tilde{\Delta}/2) - \delta_{VC}(\Delta = -\tilde{\Delta}/2) \approx \Omega^2/\tilde{\Delta}, \tag{17}$$

where δ_{VC} is given in Eq. (10).

The effective inhomogeneous width accounts for the fact that the farthest detuned velocity classes do not contribute to the EIT line shape when $\Delta_D^2 \gg \Gamma/\Omega^2\gamma$ because the EIT condition $R \gg \Gamma$ is not satisfied for these velocity classes. Far from resonance the EIT condition becomes $\Omega^2\gamma/\Delta^2 \geqslant \Gamma$, which defines a cutoff detuning $\tilde{\Delta} \approx \sqrt{\Omega^2\gamma/\Gamma}$ because the virtual transition is negligible for velocity classes with larger detunings as discussed at the end of Sec. II A [31]. If $\Delta_D^2 \ll \Gamma/\Omega^2\gamma$, then essentially all velocity classes in the Maxwellian velocity distribution contribute to EIT and the linewidth and $\tilde{\Delta} \approx \Delta_D$.

In the large-probe limit the EIT linewidth is approximately

$$\Gamma_{\mathrm{EIT}}^{LP} \approx \frac{\Omega_P\Omega_C}{\sqrt{3}\gamma}, \tag{18}$$

and the functional form of the EIT line shape is

$$\alpha^{(LP)} \propto |\delta_R|/\sqrt{\delta_R^2 + (\Omega_P\Omega_C/4\gamma_\perp)^2}, \tag{19}$$

which is a V shape. This line shape is derived in Eq. (B17) of Appendix B. To understand this linewidth we consider that in the large-probe limit the absorption due to the virtual transition decreases for large detunings Δ as indicated by Eq. (11). This decrease in absorption can be quantified by defining the absorption "area" as the integral of absorption as a function of Raman detuning. The ratio between the absorption "areas" in the large-and weak-probe limits is

$$A^{LP}/A^{WP} \approx \gamma\Omega^2/2\Omega_P\Omega_C|\Delta| = 2\gamma_\perp|\delta_{VC}|/\Omega_P\Omega_C, \tag{20}$$

where the same detuning Δ and bright Rabi frequency Ω were used in both large- and weak-probe calculations, but the Rabi frequencies Ω_P and Ω_C in Eq. (20) are the large-probe values. Equation (20) shows that relative to the weak probe limit, absorption in the large-probe limit decreases linearly as

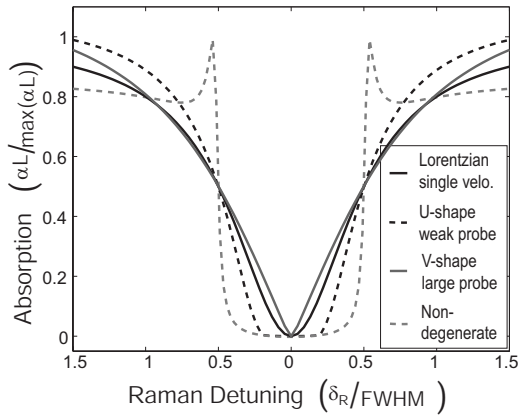

FIG. 5. Absorption line shapes for the probe field in different regimes of EIT. The solid-black curve is a perfect Lorentzian corresponding to a single velocity system. The solid-gray and dashed-black curves show, respectively, the large-probe and weak-probe limits for the case of degenerate ground states and Doppler broadening with $N_v=40$. Finally, the dashed-gray curve is for nondegenerate ground states in the weak-probe limit with probe ground state having a larger energy than the coupling ground state. All curves assume single photon resonance and $\Gamma=0$.

a function of Raman detuning δ_{VC}. Whereas in the weak-probe limit the superposition of absorption for different velocity classes sums to a constant absorption over the range $\Omega^2/\tilde{\Delta} \geqslant |\delta_R| \geqslant \Omega^2/\gamma_\perp$, in the large-probe limit the absorption becomes a linear function of the Raman detuning over this range, i.e., $\alpha \propto 2\gamma|\delta_R|/\Omega_P\Omega_C$ as indicated by Eq. (20). Finally, the large-probe EIT linewidth (HWHM) will be given by the Raman detuning for which the ratio in Eq. (20) is equal to a half, i.e., $\Gamma_{\mathrm{EIT}}/2 \approx \Omega_P\Omega_C/4\gamma$.

Figure 5 compares the line shapes for the three cases we have discussed so far: the single-velocity class Lorentzian line shape, the weak-probe *U* line shape, and the large-probe *V* line shape (the Raman detuning for each line shape has been normalized by its own FWHM). Figure 5 also shows a line shape for Doppler broadened EIT with nondegenerate ground states.

As many EIT systems have nondegenerate ground states this case merits some discussion. There are actually two different cases to consider for nondegenerate ground states depending on whether the ground state of the probe has a higher or lower energy than the coupling ground state. When $\Delta_{23}>0$ the EIT linewidth becomes larger than for the degenerate case $\Delta_{23}=0$, and the absorption can have peaks similar to those shown in Fig. 5. When $\Delta_{23}<0$ the EIT linewidth is narrower than the degenerate EIT linewidth, and in certain cases the transparency resonance can disappear entirely. These effects are most pronounced in the weak-probe case, which is the case plotted in Fig. 5.

For nondegenerate systems the expression for the virtual-transition center is

$$\delta_{VC}(\Delta) \approx \frac{\Omega_C^2}{\Delta} + \frac{\Delta\Delta_{23}}{\omega_0}, \tag{21}$$

where the second term on the right-hand side is due to the Doppler shift of the ground state frequency difference and we have assumed $\Delta(v=0)=0$ and $\omega_0 \gg \Delta_{23}$. This second term makes the Doppler broadened linewidth broader when Δ_{23} is positive, and narrower when Δ_{23} is negative. When the Rabi frequency is large, i.e., $\Omega_c \gg \tilde{\Delta}\sqrt{|\Delta_{23}|/\omega_0}$, the change in linewidth due to nondegenerate ground states is small.

When the Rabi frequency is small, i.e., $\Omega_c \sim \tilde{\Delta}\sqrt{|\Delta_{23}|/\omega_0}$, there are two different effects that occur depending on the sign of Δ_{23}. First, if Δ_{23} is positive then Eq. (21) has a minimum at $\Delta=\pm\Omega_C\sqrt{\omega_0/\Delta_{23}}$, and the FWHM of the transparency becomes $\Gamma_{\mathrm{EIT}} \approx 4|\Omega_C|\sqrt{\Delta_{23}/\omega_0}$. Also, there will be absorption spikes near $\delta_R=\pm 2|\Omega_C|\sqrt{\Delta_{23}/\omega_0}$ as seen in Fig. 5. Second, when $\Delta_{23}<0$ Eq. (21) has no minima, and the peaks of far-detuned virtual transitions can span the entire range of Raman detunings including $\delta_R=0$, effectively erasing the transparency resonance.

Although these more exotic EIT line shapes for nondegenerate ground states are interesting, they are not particularly relevant to our discussion of EIT line shapes in optically thick media. This is because the nondegenerate ground state line shapes we have discussed are only prominent in non-VCCPC systems in the weak-probe limit, and in this limit the optically thin and optically thick line shapes are essentially identical as is discussed in Sec. III.

C. Velocity changing coherence preserving collisions

The EIT line shape of Doppler broadened systems can change significantly when a buffer gas or wall coatings are used (see Fig. 6). Buffer gasses and wall coatings are used primarily to reduce decoherence Γ due to transit-time broadening. In addition to decreasing ground state decoherence, collisions between EIT atoms and the buffer gas and/or coated walls cause the atoms to change velocity classes without losing their ground state coherence. These velocity-changing coherence-preserving collisions (VCCPCs) enable the diffusion of ground state coherence from the resonant velocity classes, where the optical pumping rate is largest, to the far detuned velocity classes where optical pumping is slow. This diffusion results in two effects: there is no longer a cutoff detuning $\tilde{\Delta}$ due to decoherence effects and the inhomogeneous Doppler broadened line becomes effectively one homogeneous line with atoms freely wandering among the previously distinct velocity classes.

Similar to non-VCCPC systems, in a VCCPC system each velocity class has its own dark-state preparation rate which is given by the optical pumping rate $R(\Delta)=\Omega^2\gamma_\perp/4(\Delta^2+\gamma_\perp^2)$ (we have assumed $\Omega \ll \gamma$). However, in a VCCPC system a single atom is likely to wander through all of the velocity classes in a coherence time $t=1/\Gamma$ (a condition for a system to be a VCCPC system is that the collision rate R_C must be fast enough to create a relatively uniform ground state coherence among all velocity classes, i.e., $R_C \gg \Gamma N_v$). Thus, the ground state coherence of each atom regardless of its current velocity class will have been prepared by an average optical pumping rate

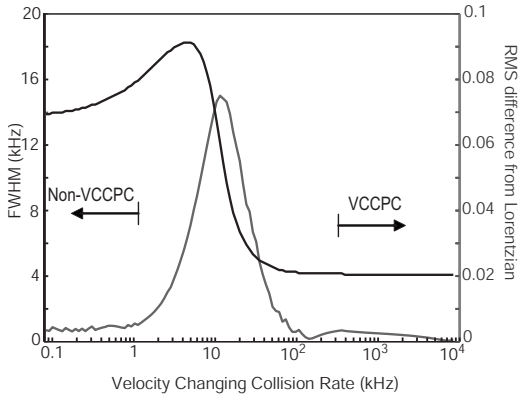

FIG. 6. EIT linewidth (black) versus the rate of velocity-changing, coherence-preserving collisions (VCCPC). The gray curve shows the rms difference between the EIT line shape and a Lorentzian line shape with the same amplitude and FWHM.

$$R_{\text{ave}} = \frac{2\sqrt{\ln 2}}{\Delta_D\sqrt{\pi}} \int_{-\infty}^{\infty} d\Delta R(\Delta) \exp(-\Delta^2 4 \ln 2/\Delta_D^2) \approx R(0)/N_v, \tag{22}$$

and the ground state coherence will be uniform across all velocity classes.

To understand the implications of a uniform ground state coherence on the EIT line shape we use the formalism of Appendix B with the simplifying assumptions $\Gamma=0$ and $\Omega_C \geqslant 10\Omega_P$ and $\Delta(v=0)=0$. Using Eq. (B8) the ground state coherence can be expressed as

$$\rho_{23} = \frac{\rho_{21}^{(-)}}{1 - i\delta_R/R_{\text{ave}}}. \tag{23}$$

Plugging Eq. (23) into Eq. (B9) from Appendix B we find that the probe susceptibility for each velocity class is

$$\chi_p(\Delta) \approx -\frac{N\mu_p^2}{2\epsilon_0\hbar}\left(\frac{-i\delta_R}{(R_{\text{ave}} - i\delta_R)(\Delta - i\gamma_\perp)}\right)^*, \tag{24}$$

where we have assumed $\delta_R \ll \gamma_\perp$. Finally, integrating over all velocity classes the Doppler averaged probe susceptibility is

$$\chi_p \approx -\mathcal{A}\frac{\delta_R}{R_{\text{ave}} + i\delta_R}, \tag{25}$$

where $\mathcal{A}$ is a constant

$$\mathcal{A} = \frac{N\gamma_\perp\mu_p^2\sqrt{\ln 2/\pi}}{2\epsilon_0\hbar\Delta_D} \int_0^{\infty} d\Delta \frac{\exp\left(-\frac{\Delta^2 4\ln 2}{\Delta_D^2}\right)}{\Delta^2 + \gamma_\perp^2} \approx \frac{N\mu_p^2}{4\epsilon_0\hbar}\frac{1}{\gamma_\perp N_v}. \tag{26}$$

Thus, the transparency line shape is a Lorentzian with a FWHM of $2R_{\text{ave}}$, which is the exact line shape we would expect from a single homogeneous line with linewidth $2N_v\gamma_\perp = \Delta_D$. Although the above derivation is for the specific case of $\Gamma=0$ and $\Delta(v=0)=0$, this result is much more general, and it can be seen empirically that EIT line shapes for VCCPC systems are very well approximated by treating the Doppler broadened line as a single velocity class with homogeneous linewidth $2N_v\gamma_\perp$ even for $\Gamma \neq 0$, $\Delta(v=0) \neq 0$, and $\Delta_{23} \neq 0$ (of course this assumption ignores the fact that Doppler-broadened line shape is Gaussian and not Lorentzian, but discrepancies resulting from this difference are typically small).

Figure 6 shows how the linewidth and line shape change as a function of the collision rate. Figure 6 also shows why the condition $R_C \gg \Gamma N_v$ must be satisfied for VCCPC systems [an exact numerical integration of Eq. (13) is used to obtain Fig. 6]. If the decoherence rate Γ is large compared to the rate of diffusion among the velocity classes ($R_C \ll \Gamma N_v$), then the ground state coherence, which is created when the atoms are in near resonant velocity classes, decays before the atoms diffuse via VCCPC to the far detuned velocity classes, and the system is considered to be non-VCCPC (in Fig. 6 this corresponds to $R_C < 1$ kHz). In order for a system to be considered VCCPC the diffusion rate must be fast compared to the decoherence rate (i.e., $R_C \gg \Gamma N_v$). Then the ground state coherence is able to diffuse to the far detuned velocity classes before it is dissipated by decoherence (in Fig. 6 this corresponds to $R_C > 100$ kHz). Also, it is interesting to note that in Fig. 6 the non-VCCPC linewidth is determined by the coherence cutoff (i.e., $\Omega\sqrt{\gamma/\Gamma} \gg \Delta_D$), but in the VCCPC region because of the coherence diffusion there is no coherence cutoff and the linewidth is $\Gamma_{\text{EIT}} = \Omega^2/\Delta_D = \Omega^2/N_v\gamma$. Finally, Fig. 6 shows that the line shape becomes essentially Lorentzian in the VCCPC limit.

III. OPTICALLY THICK MEDIA

Once we know the optically-thin EIT line shapes, it is possible to calculate the EIT line shapes in optically thick media. In general the optically thick and optically thin EIT line shapes will differ because the fields are absorbed as they propagate through the medium and, as we have already seen, the EIT line shapes depend strongly on both the absolute and relative intensities of the fields. On the other hand, the difference between the thin-medium and thick-medium EIT line shapes will be insignificant if the field or fields determining the line shape are not significantly absorbed.

This second scenario is what happens in the weak-probe limit. In the weak-probe limit the probe field is strongly absorbed for nonzero Raman detunings, but the coupling field experiences little absorption. Also, the EIT linewidth is determined primarily by the coupling Rabi frequency, not the probe. Thus, in the weak-probe limit the EIT line shape experiences almost no change as it propagates through an optically thick media, and the optically thick and optically thin line shapes are essentially the same. In contrast, in the large-probe limit the EIT line shape typically changes significantly as it propagates through an optically thick medium.

A. Optically thick line shape definitions

Before calculating the optically-thick EIT line shapes we must be more clear about what we mean by the EIT line shape. In optically thick media there are actually two definitions for the line shape, a cw EIT line shape given by Eq.

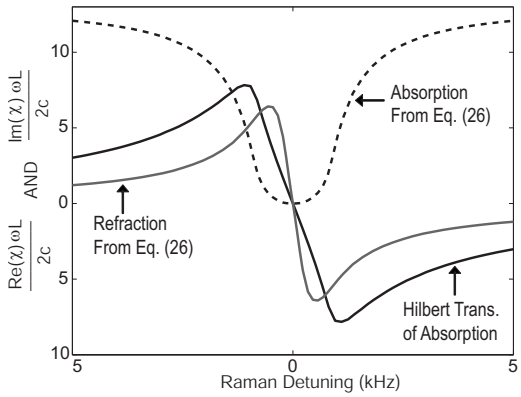

FIG. 7. Refractive (solid-gray line) and absorptive (dashed-black line) parts of the susceptibility calculated using Eq. (27) and its refractive analog. Also shown (solid-black line) is the Hilbert transform of Eq. (27). Because the refractive analog to Eq. (27) and the Hilbert transform of Eq. (27) differ significantly it is obvious that the definition for optically thick EIT line shapes given in Eq. (27) does not satisfy a Kramer's Kronig relation.

(27) and a pulsed EIT line shape given by Eq. (28). We use the cw EIT line shape as our primary definition of EIT line shape because of its experimental relevance.

Experimentally, the EIT line shape is measured by slowly scanning the frequency of a cw probe relative to the coupling frequency and measuring the probe transmission as a function of the Raman detuning. Mathematically, this EIT absorption line shape is described by

$$\alpha_1(\delta_R)L = \int_0^L dz\alpha[\Omega_C(\delta_R,z),\Omega_P(\delta_R,z),\delta_R,z], \qquad (27)$$

where $\alpha(\delta_R,\Omega_C,\Omega_P,z)=\omega_0\,\mathrm{Im}(\chi_p)/c$ is the probe absorption coefficient at position z. Similarly, the refractive analog to Eq. (27) is calculated using the same equation but with the replacement $\mathrm{Im}(\chi_p)\rightarrow\mathrm{Re}(\chi_p)$.

In spite of Eq. (27)'s experimental significance, it suffers from a couple of drawbacks with respect to pulsed EIT. For example, the refractive and absorptive parts of the susceptibility as defined in Eq. (27) do not obey Kramers Kronig relations. Figure 7 shows absorptive (dashed line) and refractive (gray line) line shapes that were calculated using Eq. (27) and its refractive analog. The optical thickness of the medium was $\alpha L=10$. The black curve in Fig. 7 is the Hilbert transform of the absorptive curve. The significant differences between the black and gray curves shows that absorption and refraction as defined by Eq. (27) do not obey Kramer's Kronig relation. This fact should not be surprising because for $z>0$ the Rabi frequencies used to calculate the local absorption (refraction) at z changes for different Raman detunings [i.e., $\Omega_C(\delta_R,z)\neq\Omega_C(\delta_R',z)$ and $\Omega_P(\delta_R,z)\neq\Omega_P(\delta_R',z)$ for $\delta_R\neq\delta_R'$ and $z>0$].

Thus, a second line shape definition is required for pulsed EIT experiments such as slow-light experiments, and the pulsed absorption line shape is

$$\alpha_2(\delta_R)L = \int_0^L dz\alpha(\Omega_C(0,z),\Omega_P(0,z),\delta_R,z), \qquad (28)$$

where the frequency distribution of the probe pulse is centered on Raman resonance with a monochromatic cw coupling field. The difference between Eqs. (27) and (28) is that in the integrand of Eq. (28) the absorption is calculated assuming the field amplitudes for Raman resonance. Equation (28) accounts for the fact that with pulses there is distribution of frequency components, and the strong near-resonant frequencies create a large ground-state coherence which reduces the absorption of the weak wing frequencies. The drawback of Eq. (28) is that it is difficult to measure experimentally. However, Eq. (28) does obey Kramer's Kronig relation, which is important for slow light experiments. Both Eqs. (27) and (28) reduce to the same definition in the limit that the medium becomes optically thin. Because of Eq. (27)'s experimental significance, and Eq. (28) lack of experimental relevance, we will always mean Eq. (27) when referring to the EIT line shape.

B. Line shapes

In the large-probe limit the EIT line shape in optically thick media changes appreciablly as a function of the propagation distance through the media. This is especially true for Doppler broadened non-VCCPC systems where the linewidth is proportional to both probe and coupling field amplitudes. The evolution of the EIT line shape in optically thick media is also significant for single-velocity class systems and VCCPC systems when $|\Omega_P|\sim|\Omega_C|$, in which case the linewidth is dependent on both the coupling and probe beams and both beams experience significant absorption as they propagate through the medium.

In steady state the amplitude of the field can be found by solving the equation

$$\frac{\partial|\Omega_P(\delta_R,z)|}{\partial z} = -\alpha(\delta_R,z)|\Omega_P(\delta_R,z)|, \qquad (29)$$

where

$$\alpha(\delta,z) \approx \alpha_0\frac{|\Omega_P|^2+C}{2|\Omega_P|^2+C}S(\delta_R,z), \qquad (30)$$

α_0 is the incoherent absorption coefficient assuming $\Omega_P\ll\Omega_C$, $S(\delta_R,z)$ is a line shape function (e.g., S will be V-shaped for Doppler broadened non-VCCPC systems), and $C=|\Omega_C|^2-|\Omega_P|^2$ is assumed to be constant with respect to z and δ_R (this assumption is justified when the dipole moments and frequencies of the probe and coupling transitions are approximately equal). In the large-probe limit there are two shape functions of interest; the V shape function for Doppler broadened non-VCCPC systems, and the Lorentzian shape function for single-velocity systems and VCCPC systems. Table I gives these two shape functions along with their respective solutions for Eq. (29). In Eq. (15) of Ref. [47] there is a line shape solution similar to the solutions for the Lorentzian shape function in Table I. The solutions to Eq. (29) are transcendental equations making them somewhat

TABLE I. Solutions to the problem of EIT line shapes and linewidths for optically thick media in the large probe limit. Two cases are considered; Doppler broadened systems and single-velocity or VCCPC systems. $\Gamma_{\mathrm{EIT}}(0)$ is the optically thin EIT linewidth FWHM. $S(\delta,z)$ is the functional form of the optically thin EIT lineshape. These line shapes are used in Eq. (29) to find the optically thick line shapes, and asymptotic expressions for these solutions are found for the limits $\delta_R \ll \Gamma_\chi(z)$ and $\delta_R > \Gamma_{\mathrm{EIT}}(0)$. Also included are approximate expressions for the coherence linewidth $\Gamma_\chi(z)$ and a lower bound for the field linewidth $\Gamma_\Omega(z)$ (both are FWHM). Some definitions used in the table are $A=|\Omega_P(0)|$. c_1 and c_2 are constants of integration and are calculated by applying the boundary condition $\Omega_P(z=0)=A$. Without loss of generality we assume that A is real.

	V shape large-probe limit with arbitrary C	Lorentzian VCCPC or single velo. with $C=0$
$\Gamma_{\mathrm{EIT}}(0)$	$\dfrac{\lvert\Omega_P\Omega_C\rvert}{\sqrt{3}\gamma}$	$\dfrac{2\lvert\Omega_P\rvert^2}{N_v\gamma}$
$1/S(\delta,z)$	$\sqrt{1+\dfrac{\lvert\Omega_P\rvert^2\lvert\Omega_C\rvert^2}{4\gamma^2\delta_R^2}}$	$1+\dfrac{\lvert\Omega_P\rvert^4}{N_v^2\gamma^2\delta_R^2}$
Eq. (29) solution	$x-\tanh^{-1}\left(\dfrac{1}{x}\right)\cdots$ $=-2\alpha_0+c_1$	$\ln\lvert\Omega_P\rvert+\dfrac{\lvert\Omega_P\rvert^4}{4N_v^2\gamma^2\delta_R^2}\cdots$ $=-\alpha_o z/2+c_2$
	$x=\left(1+\dfrac{\lvert\Omega_P\rvert^2\lvert\Omega_C\rvert^2}{4\gamma^2\delta_R^2}\right)^{1/2}$	
$\lvert\Omega_P(z)\rvert$ $[\delta \ll \Gamma_{\mathrm{EIT}}(z)]$	$A-\dfrac{4\alpha_0 z\gamma\delta_R}{\Omega_C}$	$(A^4-2\alpha_o z N_v^2\gamma^2\delta_R^2)^{1/4}$
$\lvert\Omega_P(z)\rvert$ $[\delta \gg \Gamma_{\mathrm{EIT}}(0)]$	$Ae^{-\alpha_0 z\lvert\Omega_C\rvert^2/\lvert\Omega_C\rvert^2+\lvert\Omega_P\rvert^2}$	$Ae^{-\alpha_0 z/2}$
$\dfrac{\Gamma_{\mathrm{EIT}}(0)}{\Gamma_\chi(z)}\approx$	$1+\dfrac{\alpha_0 z}{\sqrt{3}}$	$\sqrt{1+2\alpha_0 z}$
$\dfrac{\Gamma_\Omega(z)}{\Gamma_{\mathrm{EIT}}(0)}\gg$	$\dfrac{1-e^{-\alpha_0 z/2}}{\alpha_0 z/2}$	$\sqrt{\dfrac{1-e^{-2\alpha_0 z}}{2\alpha_0 z}}$

difficult to interpret. Thus, we have also included asymptomatic solutions for the limits when the Raman detuning is small compared with the EIT linewidth [i.e., $\delta_R \ll \Gamma_{\mathrm{EIT}}(z)$], and when the Raman detuning is large compared to the EIT linewidth [i.e., $\delta_R \gg \Gamma_{\mathrm{EIT}}(0)$].

The asymptotic solutions corresponding to small Raman detuning provide a basis for calculating approximate EIT linewidths as a function of position z. There are actually two linewidths to be calculated; the coherence linewidth Γ_χ, which is the FWHM of $\alpha(z)$, and the field linewidth Γ_Ω, which is the integrated absorption encountered by the field up to position z, i.e., $\int_0^z dz'\,\alpha(z')$. For optically thin media these two linewidths are the same. Because these linewidths become narrower with increasing optical depth the coherence linewidth will always be narrower than the field linewidth. The narrowness of the coherence linewidth Γ_χ allows us to

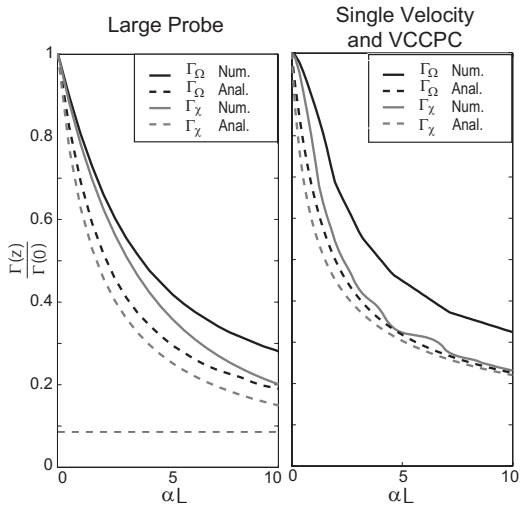

FIG. 8. Linewidths (FWHM) of the probe field (black) and coherence (gray) for the cases of a single-velocity system and a Doppler broadened system in the strong probe regime. The linewidths were calculated using the analytic expression given in Table I (dashed lines) and an exact numerical simulation of Eq. (27). For the single velocity case $\Omega_C=\Omega_P=\gamma/3$ and $\Gamma=10$ kHz. For the large probe case $\Omega_C=5\Omega_P=\gamma/8$, $\Gamma=0$, and $v_p=43c\gamma/\omega_0$.

accurately estimate it using the asymptotic solutions from Table I. We cannot accurately estimate the field linewidth Γ_Ω using the small Raman detuning asymptotic solution, but we can calculate a lower bound for the field linewidth. Both the estimate of Γ_χ and the lower bound for Γ_Ω are shown in Table I.

In Fig. 8 we compare numerical simulations of fields propagating through optically thick media with the approximate expressions for Γ_χ and the lower bound for Γ_Ω in Table I. There are two plots shown one for each line shape considered in Table I. The numerical linewidths are plotted using solid lines, and the analytic solutions from Table I are plotted using dashed lines. The gray curves show the coherence FWHMs Γ_χ and the black curves show the field FWHMs Γ_Ω. The analytic solutions seem to slightly overestimate the narrowing, and the coherence linewidths show better agreement between numerical and analytic solutions than the field linewidths, which is consistent with the field linewidth being a lower bound rather than an estimate of the linewidth. Also confirmed in Fig. 8 is the inequality $\Gamma_\chi \ll \Gamma_\Omega$. In the large probe plot the linewidths should asymptotically approach the weak-probe linewidth $\Gamma_{\mathrm{EIT}}=C/\tilde{\Delta}$, which is indicated by the thin dashed line. The numerical simulation approaches this limit. However, the analytic solutions asymptotically approaches zero because our approximations do not account for the small-probe limit. The asymptotic limit for the single velocity linewidth is $\Gamma_\chi=\Gamma_\Omega=C/N_v\gamma$.

In actual experimental systems there are additional considerations which have not been considered in this paper. First, experiments will most likely use Gaussian beams, not plane waves. The theory presented in this paper can be generalized to account for transverse variations in the field intensity by applying the above results to each transverse point $\{x,y\}$ and integrating over the beam profile (special consid-

erations are required if the Raleigh length for the beam is not much longer than the medium). Second, when the EIT ground states are not degenerate the probe and coupling fields typically create a Stark shift which changes the frequency of Raman resonance. As the fields are absorbed this displacement of Raman resonance will decrease, and the EIT linewidth and line shape will be affected. However, in almost all cases this Stark shift has little affect on the line shape because the Stark shift $\Omega^2/4\Delta_{23}$ is typically small compared to the EIT linewidth. This is because in order to obtain good EIT the ground state frequency difference Δ_{23} should be much larger than the homogeneous and inhomogeneous linewidths of the probe and coupling transitions. Thus, the effect of the Stark shift will by minimal and can be ignored. Finally, the diffusion of atoms in and out of the beams in VCCPC systems can have some interesting effects on the EIT line shape when Gaussian beams are considered [49–51]. However, our description of VCCPC systems is adequate for most cases, and a more detailed model is beyond the scope of this paper.

IV. CONCLUSION

The EIT linewidths and line shapes can change significantly when going from an optically thin medium to an optically thick medium. The difference is that in optically thick medium the absorption of the fields as they propagate through the medium leads to changes in the EIT linewidth and line shape as a function of optical depth. This results from the dependence of the EIT line shape on the field amplitudes. The differences between optically thick and optically thin line shapes are primarily encountered in the large-probe limit. The linewidth will decrease as a function of propagation distance until it reaches an asymptotic value as discussed in Sec. III B. These results are limited to cw EIT experiments, and we have discussed the differences between the cw and pulsed EIT line shapes in optically thick media.

We have also discussed the factors influencing the EIT line shapes in optically thin media. Although EIT linewidths in different types of optically thin media have been well characterized, the line shapes had received less attention. Near single-photon resonance single velocity systems and VCCPC systems have Lorentzian line shapes, whereas Doppler broadened non-VCCPC systems have *V* shaped transparency resonances in the large-probe limit and *U* shaped resonances in the weak-probe limit. Here we only consider EIT line shapes near single-photon resonance, but off resonance line shapes have been studied elsewhere [35].

In the interest of simplicity we have not included all possible effects encountered in the lab. For example, we have not looked at effects due to transverse inhomogeneities in the field intensities.

ACKNOWLEDGMENTS

This work was supported by DARPA Slow Light, the National Science Foundation, and Research Corporation.

APPENDIX A: ANALYTIC EIT LINE SHAPES FOR THE WEAK-PROBE LIMIT

In the weak-probe limit we can use perturbation theory to solve Eq. (1) in the steady state. We solve the master equation, given in Eq. (1), by rearranging the density matrix into a vector

$$\vec{\rho} = [\rho_{11},\rho_{22},\rho_{33},\mathrm{Re}(\rho_{21}),\mathrm{Im}(\rho_{21}),\ldots,\mathrm{Re}(\rho_{32}),\mathrm{Im}(\rho_{32}),\mathrm{Re}(\rho_{31}),\mathrm{Im}(\rho_{31})]^T,$$

such that the master equation becomes a simple matrix equation

$$\dot{\vec{\rho}} = (M + \Omega_P P)\vec{\rho}, \tag{A1}$$

where P is a matrix accounting for all terms from Eq. (1) proportional to the probe field Ω_P, and all the remaining terms in the master equation are included in the matrix M. The steady-state solution is found by setting the time derivatives to zero, replacing one of the rows corresponding to either $\dot{\rho}_{11}$, $\dot{\rho}_{22}$, or $\dot{\rho}_{33}$ with the normalization condition $\rho_{11}+\rho_{22}+\rho_{33}=1$, and solving to obtain

$$\vec{\rho}^{(ss)} = (\tilde{M} + \Omega_P \tilde{P})^{-1}\vec{v}, \tag{A2}$$

where the tildes denote that the matrices have been modified to include the normalization condition and $\vec{v} = [1,0,0,0,0,0,0,0,0]^T$ arises from the 1 on the right-hand side of the normalization condition.

The perturbative solution is found by defining the steady-state solution as

$$\vec{\rho}^{(ss)} = \sum_{n=0}^{\infty} \epsilon^n \vec{\rho}_n \tag{A3}$$

and writing the steady state matrix equation as

$$(\tilde{M} + \epsilon\Omega_P \tilde{P})\sum_{n=0}^{\infty} \epsilon^n \vec{\rho}_n = \vec{v}. \tag{A4}$$

By collecting terms with the same power of ϵ and setting $\epsilon = 1$ it is found that the perturbation solutions are

$$\vec{\rho}_0 = \tilde{M}^{-1}\vec{v}, \tag{A5a}$$

$$\vec{\rho}_n = (-\Omega_P)^n(\tilde{M}^{-1}\tilde{P})^n\vec{\rho}_0. \tag{A5b}$$

Most perturbative treatments of EIT, including this paper, use the first order perturbative solution, i.e., $\vec{\rho} \approx \vec{\rho}_0 + \vec{\rho}_1$ [31,33,40,41]. This solution is valid to first order in the probe and to all orders in all other parameters. The perturbation solution suffers from the fact that for large single-photon detunings the perturbation series in Eq. (A3) does not converge unless the probe Rabi frequency is many orders of magnitude smaller than coupling Rabi frequency.

APPENDIX B: ANALYTIC EIT LINE SHAPES FOR THE LARGE-PROBE LIMIT

It is possible to derive an analytic expression for the probe susceptibility without the assumption of a weak probe by

using the Bloch-vector formalism of Benink [11]. The Bloch-vector formalism assumes that the coherences from the ground states to the excited state can be adiabatically eliminated and makes no assumptions about the relative strengths of the probe and coupling fields. The Bloch-vector formalism is ideal for analyzing Doppler-broadened EIT line shapes in the large-probe limit because the far-detuned velocity classes which make the largest contributions to the Doppler-broadened EIT line shapes strongly satisfy the criterion for adiabatic elimination.

By adiabatically eliminating the excited state coherences the density matrix can be rewritten as a Bloch-vector equation for the two ground states

$$\frac{d}{dt}\vec{\rho} = (R+\Gamma)[-\vec{\rho} + \vec{T}\times\vec{\rho} + (1-3\rho_{11})\vec{F}], \tag{B1}$$

and a first-order differential equation for the excited state population

$$\frac{d}{dt}\rho_{11} = -\gamma\rho_{11} - (R+\Gamma)\vec{\rho}\cdot\vec{F} + (1-3\rho_{11})R. \tag{B2}$$

In the above we have used the following definitions

$$\vec{\rho} = \begin{pmatrix} u \\ v \\ w \end{pmatrix} = \begin{pmatrix} 2\,\mathrm{Re}(\rho_{23}) \\ 2\,\mathrm{Im}(\rho_{23}) \\ \rho_{22}-\rho_{33} \end{pmatrix}, \tag{B3}$$

$$\vec{F} = -\frac{R/\Omega^2}{R+2\Gamma_\perp}\begin{pmatrix} 2\Omega_P\Omega_C \\ 0 \\ \Omega_P^2-\Omega_C^2 \end{pmatrix}, \tag{B4}$$

$$\vec{T} = \bar{\delta}\hat{w} + \frac{\Delta}{\gamma_\perp}\vec{F}, \tag{B5}$$

$$R = \frac{\Omega^2\Gamma_\perp/4}{\Delta^2+\Gamma_\perp^2}, \tag{B6}$$

where $\hat{w}=(0,0,1)^T$ is the unit vector in the direction of w, $\bar{\delta}=\delta_R/(R+\Gamma_\perp)$, and it is assumed that both Ω_P and Ω_C are real.

By assuming a large single-photon detuning Δ and assuming the fields are well below saturation (i.e., $\gamma_\perp \gg \Omega_C \gg \Omega_P$), the population in the excited state will always be negligible $\rho_{11}\approx 0$, which allows further simplification of the problem by setting $\rho_{11}=0$. In this case the steady state solution of Eq. (B1) becomes

$$\vec{\rho}^{ss} = \vec{F} + \frac{F_u\bar{\delta}}{1+T^2}\left[-\hat{u}\left(\bar{\delta}+\frac{F_w\Delta}{\gamma}\right) + \hat{v} + \hat{w}F_u\frac{\Delta}{\gamma}\right], \tag{B7}$$

where $T^2=\|\vec{T}\|^2$. Also, the ground state coherence is

$$\rho_{23} = \frac{F_u}{2}\left\{1 + \frac{\bar{\delta}}{1+T^2}\left[i - \left(\bar{\delta}+\frac{F_w\Delta}{\gamma}\right)\right]\right\}. \tag{B8}$$

In adiabatically eliminating the excited state coherences one finds that the coherence along the probe transition ($|1\rangle\leftrightarrow|2\rangle$) is given by

$$\rho_{12} \approx -\frac{\Omega_P\rho_{22}}{2}\frac{1+\rho_{23}^*\Omega_C/\rho_{22}\Omega_P}{\Delta-\delta/2+i\gamma_\perp} \approx -\frac{\Omega_P\rho_{22}}{2}\left(\frac{1-\rho_{23}/\rho_{23}^{(-)}}{\Delta-\delta/2-i\gamma_\perp}\right)^*, \tag{B9}$$

where the assumption $\rho_{22}\approx|\Omega_C|^2/\Omega^2$ and the identity $\rho_{23}=-\Omega_P^*\Omega_C/\Omega^2$ have been used in the last line. Finally, the probe susceptibility is given by

$$\chi_p = \frac{N\mu_p^2}{\epsilon_0\hbar}\frac{\rho_{12}}{\Omega_P} \approx -\frac{N\mu_p^2\rho_{22}}{2\epsilon_0\hbar}\left[\frac{\Gamma_\perp + \frac{\bar{\delta}R}{1+T^2}(-i+\bar{\delta}+F_w\Delta/\gamma)}{(R+\Gamma_\perp)(\Delta-\delta_R/2-i\gamma_\perp)}\right]^*, \tag{B10}$$

where the identity $F_u=2R\rho_{23}^{(-)}/(R+\Gamma_\perp)$ has been used in the last line.

Our primary interest is the absorption line shape which is given by the imaginary part of the susceptibility

$$\mathrm{Im}(\chi_p) \approx \frac{N\mu_p^2\rho_{22}}{2\epsilon_0\hbar}\frac{2\Gamma_\perp\gamma_\perp + \frac{\bar{\delta}R}{1+T^2}[\Delta(F_w-1)+\gamma_\perp\bar{\delta}]}{(R+\Gamma_\perp)(\Delta^2+\gamma_\perp^2)}. \tag{B11}$$

Although Eq. (B11) is not overly complicated, when analyzing the absorption line shape it is helpful to simplify by considering the limit in which $\Gamma_\perp=0$ and $F_w\approx 1$, such that the imaginary part of the susceptibility can be written as

$$\mathrm{Im}(\chi_p) \approx \frac{32N\sigma_p\delta_R^2\gamma_\perp^2\left(\frac{\Delta^2}{\gamma_\perp^2}+1\right)}{\Omega^4\left[\left(\frac{4\delta_R(\Delta^2+\gamma_\perp^2)}{\Omega^2\gamma_\perp}-\frac{\Delta}{\gamma_\perp}\right)^2+\left(F_u^2\frac{\Delta^2}{\gamma_\perp^2}+1\right)\right]}, \tag{B12}$$

where we have defined $\sigma_p=\mu_p^2/4\epsilon_0\hbar\gamma_\perp$ and we have used the definition of the optical pumping rate $R=\Omega^2\gamma_\perp/4(\Delta^2+\gamma_\perp^2)$. In the limit of large single-photon detunings Eq. (B12) describes a "virtual" absorption peak centered at $\Omega^2/2\Delta$ with a peak height of

$$h = 2N\sigma_p/(1+F_u^2\Delta^2/\gamma_\perp^2)$$

and the FWHM is

$$w = \Omega^2\gamma_\perp\sqrt{1+F_u^2\Delta^2/\gamma_\perp^2}/4\Delta^2.$$

Also, on Raman resonance Eq. (B12) exhibits the Lorentzian-like transparency resonance expected for EIT.

The Doppler averaged absorption line is obtained by integrating over the Maxwellian velocity distribution similar to Eq. (13)

$$\mathrm{Im}(\chi_p) = \frac{2\sqrt{\ln 2}}{\sqrt{\pi}\Delta_D}\int_{-\infty}^{\infty} d\Delta\ \mathrm{Im}[\chi_p(\Delta)]\exp\left(-\frac{\Delta^2 4\ln 2}{\Delta_D^2}\right). \tag{B13}$$

Because the far-detuned virtual transitions are very narrow, they can be reasonably approximated by delta functions cen-

tered at $\delta_R=\Omega^2/4\Delta$ with the same area as the approximately Lorentzian virtual transitions

$$A(\Delta) \approx \frac{\pi}{2} hw \approx \pi N \sigma_p \Omega^2 \gamma_\perp / 4\Delta^2 \sqrt{1 + F_u^2 \Delta^2 / \gamma_\perp^2}. \tag{B14}$$

With this approximation the Doppler averaged absorption line becomes

$$\begin{aligned} \mathrm{Im}(\chi_p) &\approx \int_{-\infty}^{\infty} d\Delta \frac{A(\Delta) \exp\left(- \frac{\Delta^2 4 \ln 2}{\Delta_D^2} \right) \delta\left(\delta_R - \frac{\Omega^2}{4\Delta} \right)}{\Delta_D \sqrt{\pi / \ln 2}/2} \\ &\approx \frac{2 N \sigma_p \gamma_\perp \sqrt{\pi \ln 2} \exp\left(- \frac{\ln 2 \Omega^4}{4 \delta_R^2 \Delta_D^2} \right)}{\Delta_D \sqrt{1 + F_u^2 \Omega^4 / 16 \delta_R^2 \gamma_\perp^2}}. \end{aligned} \tag{B15}$$

This expression for the Doppler averaged line shape is valid for both the large-probe limit ($F_u \Delta_D / \gamma_\perp \geq 1$) and the weak-probe limit ($F_u \Delta_D / \gamma_\perp < 1$) where we have assumed that the Doppler width Δ_D is at least an order of magnitude larger than the homogeneous linewidth $2\gamma_\perp$. When the weak-probe limit is well satisfied (i.e., $F_u \Delta_D / \gamma_\perp \ll 1$) the line shape simplifies to

$$\mathrm{Im}(\chi_p) \approx \frac{2 N \sigma_p \gamma_\perp \sqrt{\pi \ln 2}}{\Delta_D} \exp\left(- \frac{\ln 2 \Omega^4}{4 \delta_R^2 \Delta_D^2} \right), \tag{B16}$$

and the FWHM of the transparency is Ω^2/Δ_D, which is the same result as given in Eq. (14). In the extreme large-probe limit the line shape becomes

$$\mathrm{Im}(\chi_p) \approx \frac{2 N \sigma_p \gamma_\perp \sqrt{\pi \ln 2}}{\Delta_D \sqrt{1 + F_u^2 \Omega^4 / 16 \delta_R^2 \gamma_\perp^2}}. \tag{B17}$$

with a FWHM given by $\Omega_P \Omega_C / \gamma_\perp \sqrt{3}$, which is the same result as given in Eq. (18).

These derivation become substantially more complicated for a nonzero ground state decoherence rate. However, we have found empirically through numerical experimentation that for moderate ground state decoherence rates $10\Gamma_\perp \leq \Omega^2/\gamma_\perp$ the FWHM of the large-probe transparency is approximately given by

$$\mathrm{FWHM} = \frac{\Omega_P \Omega_C}{\gamma_\perp \sqrt{3}} \left(1 + 2 \frac{\sqrt{\Gamma_\perp \gamma_\perp}}{\Omega_C} \right).$$

The authors do not have a clear explanation for the physical mechanism responsible for this particular functional form. Discussion of the line shapes and linewidths in the weak-probe limit with nonzero ground state decoherence is found in Sec. II B of the text.

[1] A. Kasapi, M. Jain, G. Y. Yin, and S. E. Harris, Phys. Rev. Lett. **74**, 2447 (1995).
[2] M. M. Kash, V. A. Sautenkov, A. S. Zibrov, L. Hollberg, G. R. Welch, M. D. Lukin, Y. Rostovtsev, E. S. Fry, and M. O. Scully, Phys. Rev. Lett. **82**, 5229 (1999).
[3] L. Hau, S. Harris, Z. Dutton, and C. Behroozi, Nature (London) **397**, 594 (1999).
[4] M. Fleischhauer and M. D. Lukin, Phys. Rev. Lett. **84**, 5094 (2000).
[5] C. Liu, Z. Dutton, C. H. Behroozi, and L. V. Hau, Nature (London) **409**, 490 (2001).
[6] V. Balić, D. A. Braje, P. Kolchin, G. Y. Yin, and S. E. Harris, Phys. Rev. Lett. **94**, 183601 (2005).
[7] R. G. Beausoleil, W. J. Munro, and T. P. Spiller, J. Mod. Opt. **51**, 1559 (2004).
[8] S. E. Harris, J. E. Field, and A. Imamoğlu, Phys. Rev. Lett. **64**, 1107 (1990).
[9] M. Jain, H. Xia, G. Y. Yin, A. J. Merriam, and S. E. Harris, Phys. Rev. Lett. **77**, 4326 (1996).
[10] Y.-Q. Li and M. Xiao, Opt. Lett. **21**, 1064 (1996).
[11] R. S. Bennink, Ph.D. thesis, University of Rochester, Institute of Optics, Rochester, 2004.
[12] D. A. Braje, V. Balić, S. Goda, G. Y. Yin, and S. E. Harris, Phys. Rev. Lett. **93**, 183601 (2004).
[13] M. O. Scully and M. Fleischhauer, Phys. Rev. Lett. **69**, 1360 (1992).
[14] M. Fleischhauer and M. O. Scully, Phys. Rev. A **49**, 1973 (1994).
[15] R. Wynands and A. Nagel, Appl. Phys. B **68**, 1 (1999).
[16] P. Hemmer, S. Ezekiel, and J. C. C. Leiby, Opt. Lett. **8**, 440 (1983).
[17] J. Kitching, S. Knappe, N. Vukičević, L. Hollberg, R. Wynands, and W. Weidemann, IEEE Trans. Instrum. Meas. **49**, 1313 (2000).
[18] P. R. Hemmer, D. P. Katz, J. Donoghue, M. Cronin-Golomb, M. S. Shahriar, and P. Kumar, Opt. Lett. **20**, 982 (1995).
[19] H. Schmidt and A. Imamoğlu, Opt. Lett. **21**, 1936 (1996).
[20] S. E. Harris and Y. Yamamoto, Phys. Rev. Lett. **81**, 3611 (1998).
[21] E. Paspalakis and P. L. Knight, J. Mod. Opt. **49**, 87 (2002).
[22] R. W. Boyd and D. J. Gauthier, *Progress in Optics* (Elsevier Science, Amsterdam, 2002), Vol. 43, Chap. 6, p. 275.
[23] M. V. Pack, R. M. Camacho, and J. C. Howell, Phys. Rev. A **74**, 013812 (2006).
[24] M. Lindberg and R. Binder, Phys. Rev. Lett. **75**, 1403 (1995).
[25] J. Gea-Banacloche, Y. Q. Li, S.-Z. Jin, and M. Xiao, Phys. Rev. A **51**, 576 (1995).
[26] H. Y. Ling, Y.-Q. Li, and M. Xiao, Phys. Rev. A **53**, 1014 (1996).
[27] S. Brandt, A. Nagel, R. Wynands, and D. Meschede, Phys. Rev. A **56**, R1063 (1997).
[28] M. D. Lukin, M. Fleischhauer, A. S. Zibrov, H. G. Robinson, V. L. Velichansky, L. Hollberg, and M. O. Scully, Phys. Rev. Lett. **79**, 2959 (1997).
[29] A. V. Taĭchenachev, A. M. Tumaikin, and V. I. Yudin, JETP Lett. **72**, 119 (2000).
[30] M. Erhard and H. Helm, Phys. Rev. A **63**, 043813 (2001).
[31] S. E. Harris and Y. Yamamoto, Phys. Rev. Lett. **81**, 3611

(1998).
[32] C. Y. Ye and A. S. Zibrov, Phys. Rev. A **65**, 023806 (2002).
[33] Y. Rostovtsev, I. Protsenko, and H. Lee, J. Mod. Opt. **49**, 2501 (2002).
[34] A. V. Taĭchenachev, V. I. Yudin, R. Wynands, M. Stahler, J. Kitching, and L. Hollberg, Phys. Rev. A **67**, 033810 (2003).
[35] S. Knappe, M. Stähler, C. Affolderbach, A. V. Taĭchenachev, V. I. Yudin, and R. Wynands, Appl. Phys. B **76**, 57 (2003).
[36] E. Arimondo, *Progress in Optics* (Elsevier Science, Amsterdam, 1996), Vol. 35, p. 275.
[37] J. P. Marangos, J. Mod. Opt. **45**, 471 (1998).
[38] S. Alam, *Lasers Without Inversion and Electromagnetically Induced Transparency* (SPIE, Washington, 1999).
[39] M. Fleischhauer, A. Imamoğlu, and J. P. Marangos, Rev. Mod. Phys. **77**, 633 (2005).
[40] H. Lee, Y. Rostovtsev, C. J. Bednar, and A. Javan, Appl. Phys. B **76**, 33 (2003).
[41] M. O. Scully and M. S. Zubairy, *Quantum Optics* (Cambridge University Press, Cambridge, 1997).
[42] M. Fleischhauer, Opt. Express **4**, 107 (1999).
[43] A. B. Matsko, I. Novikova, M. O. Scully, and G. R. Welch, Phys. Rev. Lett. **87**, 133601 (2001).
[44] E. Figueroa, F. Vewinger, J. Appel, and A. I. Lvosky, Opt. Lett. **31**, 2625 (2006).
[45] S. M. Rochester and D. Budker, J. Mod. Opt. **49**, 2543 (2002).
[46] F. Levi, A. Godone, J. Vanier, S. Micalizio, and G. Modugno, Eur. Phys. J. D **12**, 53 (2000).
[47] A. Godone, F. Levi, S. Micalizio, and J. Vanier, Eur. Phys. J. D **18**, 5 (2002).
[48] A. Godone, F. Levi, and S. Micalizio, Phys. Rev. A **65**, 033802 (2002).
[49] E. Pfleghaar, J. Wurster, S. I. Kanorsky, and A. Weis, Opt. Commun. **99**, 303 (1993).
[50] A. V. Taĭchenachev, A. M. Tumaikin, V. I. Yudin, M. Stähler, R. Wynands, J. Kitching, and L. Hollberg, Phys. Rev. A **69**, 024501 (2004).
[51] Y. Xiao, I. Novikova, D. F. Phillips, and R. L. Walsworth, Phys. Rev. Lett. **96**, 043601 (2006).